

Supporting Information

Efficient Iodine Capture from Water Using a Functionalized Covalent Organic Framework

Mahsa Jahantigh,¹ Mostafa Khajeh,^{1,*} Ali Reza Oveisi,^{2,*} Saba Daliran,² and Mansoureh Rakhshanipour¹

¹ Department of Chemistry, Faculty of Sciences, University of Zabol, P.O. Box: 98615-538, Zabol, Iran

² Department of Organic Chemistry, Faculty of Chemistry, Lorestan University, Khorramabad 68151-44316, Iran.

Corresponding authors:

E-mail: m_khajeh@uoz.ac.ir (M. Khajeh) and oveisi.a@lu.ac.ir (A. R. Oveisi), Fax: +98-543-2226765

Instruments

PerkinElmer Spectrum spectrometer (Version 10.01.00) with KBr pellet preparation was used to acquire Fourier-transform infrared (FT-IR) spectra. Diffraction analysis was carried out using a Philips X'Pert diffractometer (Cu K α radiation, $\lambda = 1.5406 \text{ \AA}$). To determine the elemental composition of the samples, energy-dispersive X-ray spectroscopy (EDX) was employed using a TESCAN MIRA3 field-emission scanning electron microscope (FE-SEM). UV-Vis absorption measurements were conducted on an Agilent 8453 spectrophotometer at $\lambda = 458 \text{ nm}$ to monitor iodine concentration in the supernatant solution over time. The thermal stability of the samples was evaluated by thermogravimetric analysis (TGA) using a Mettler Toledo TGA/DSC instrument. Measurements were conducted from ambient temperature to $700 \text{ }^\circ\text{C}$ under air constant heating rate of $10 \text{ }^\circ\text{C}/\text{min}$. Nitrogen physisorption measurements were performed at 77 K using a Micromeritics TriStar II Plus surface area and porosity analyzer. Prior to analysis, the samples were degassed under vacuum at $120 \text{ }^\circ\text{C}$ for 12 hours. Raman spectra were collected using an RM2000 confocal Raman spectrometer.

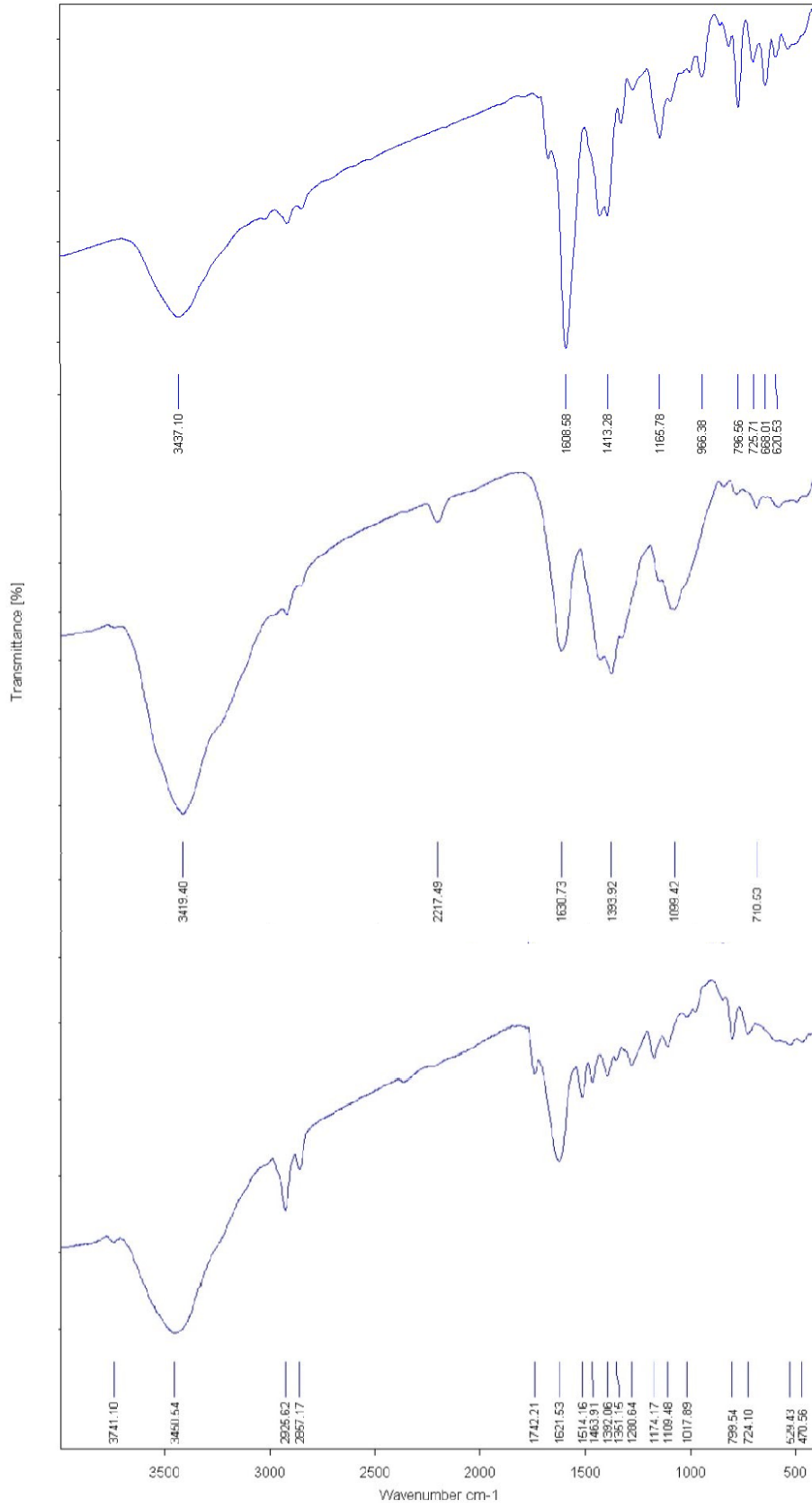


Figure S1. Comparative FT-IR spectra: COF-366 (top), COF-366-CN (middle), and POP-AO (bottom).

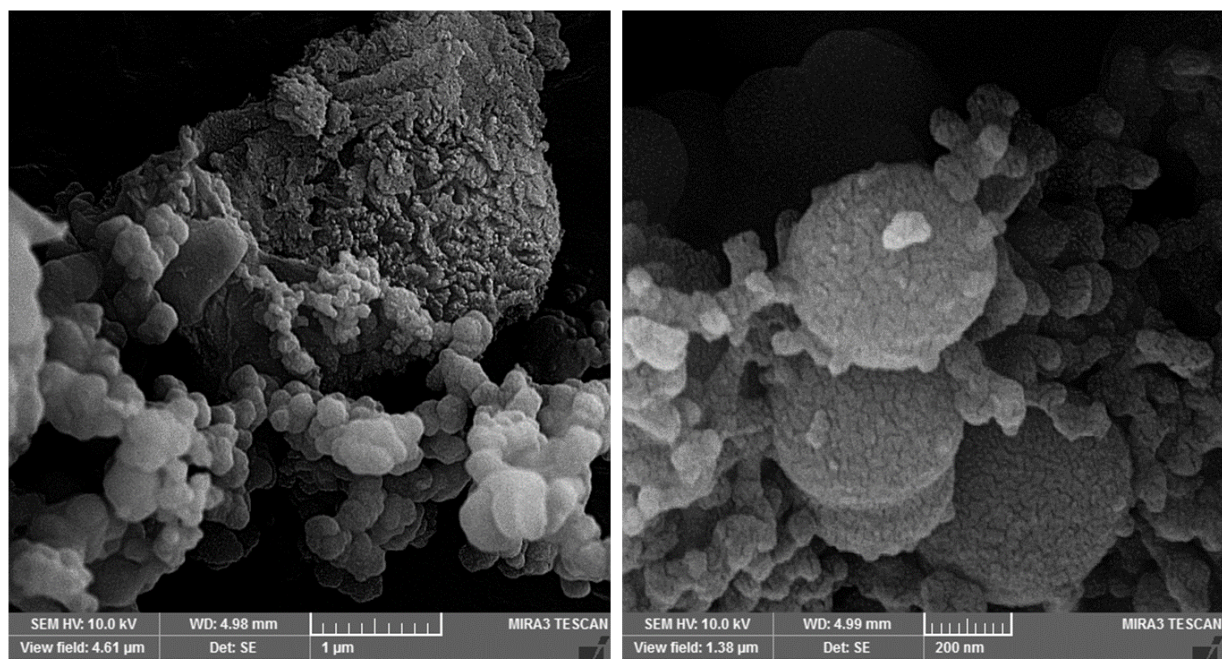


Figure S2. SEM images of COF-366 at different magnifications.

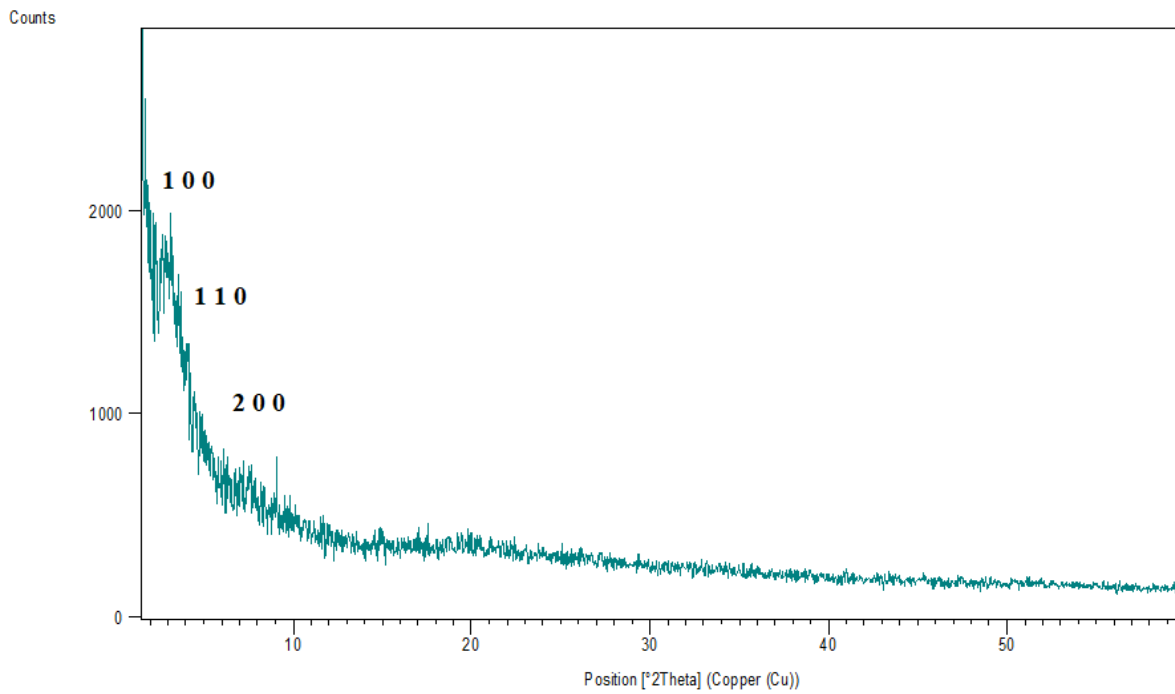


Figure S3. XRD pattern of COF-366.

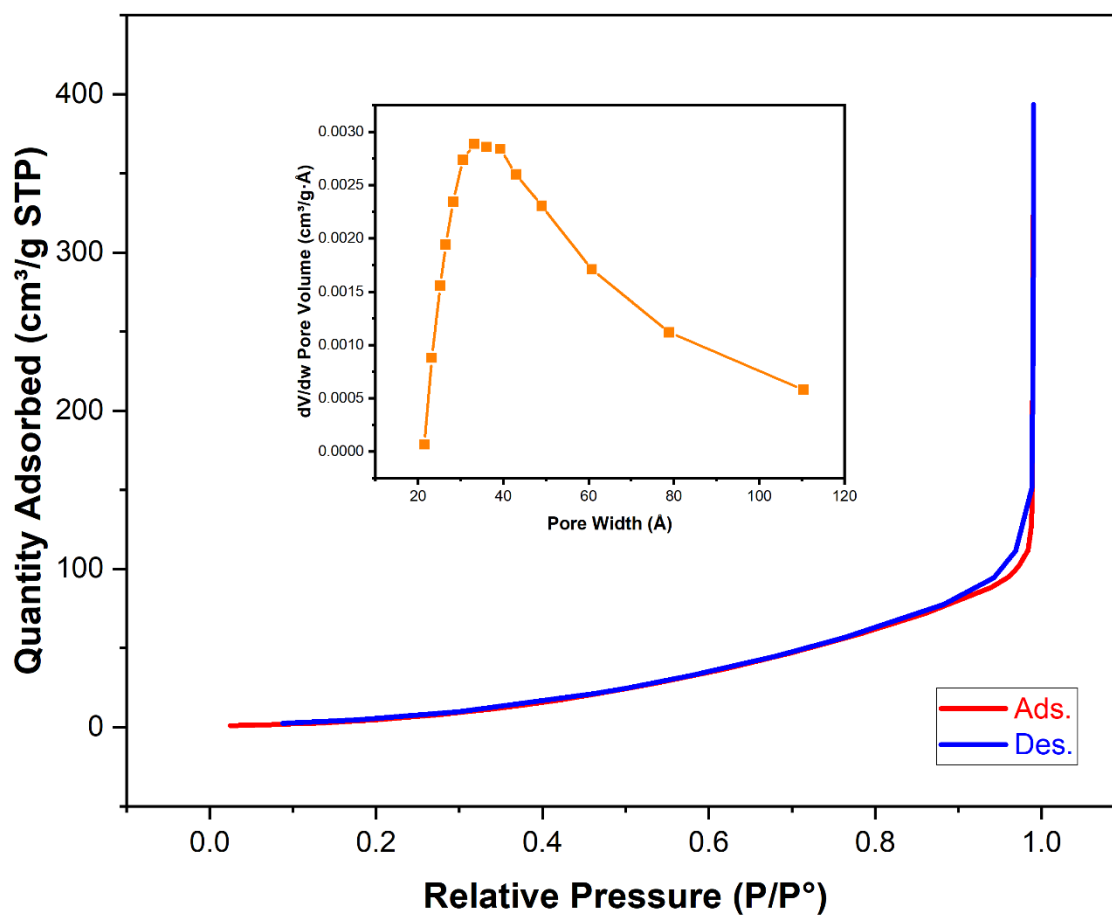


Figure S4. Nitrogen adsorption-desorption isotherm for POP-AO; the corresponding pore size distribution plot is shown in the inset.

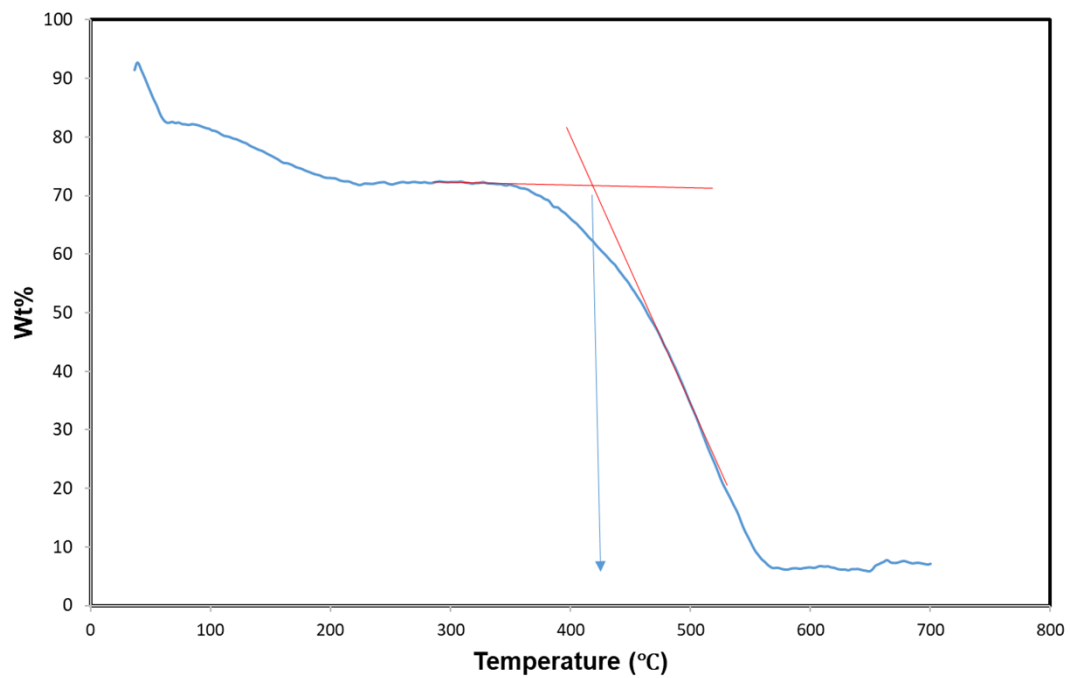


Figure S5. TGA profile for POP-AO, showing mass loss as a function of temperature.

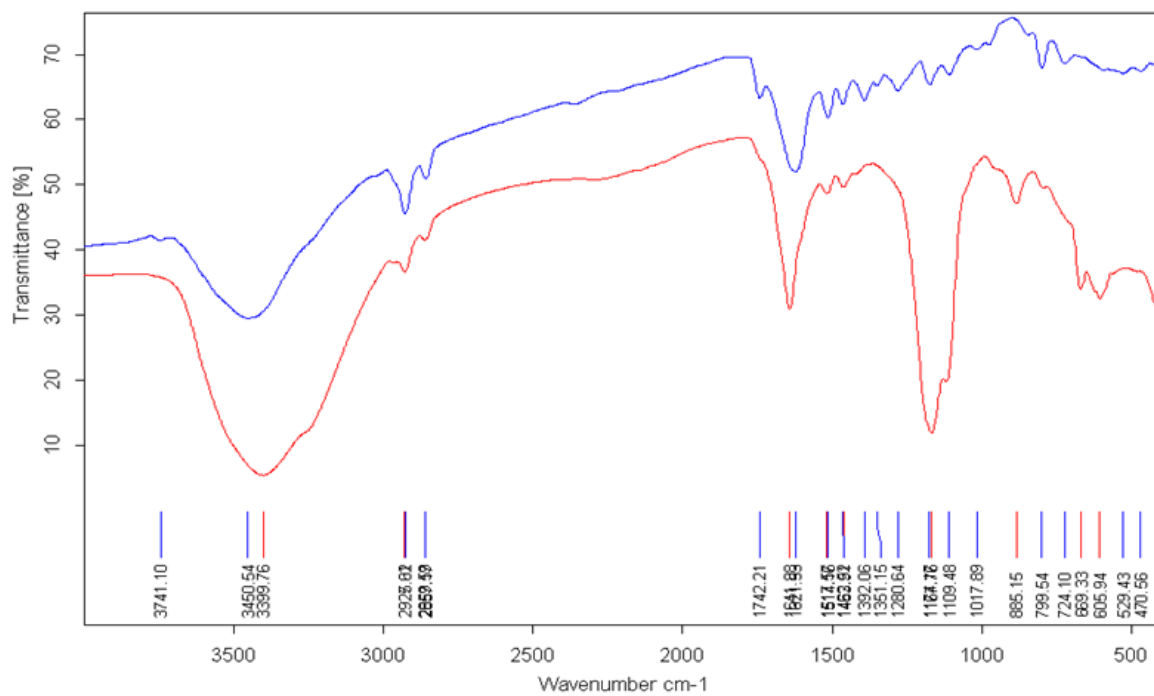


Figure S6. FT-IR spectra of POP-AO (top, blue) and POP-AO-I₂ (bottom, red).

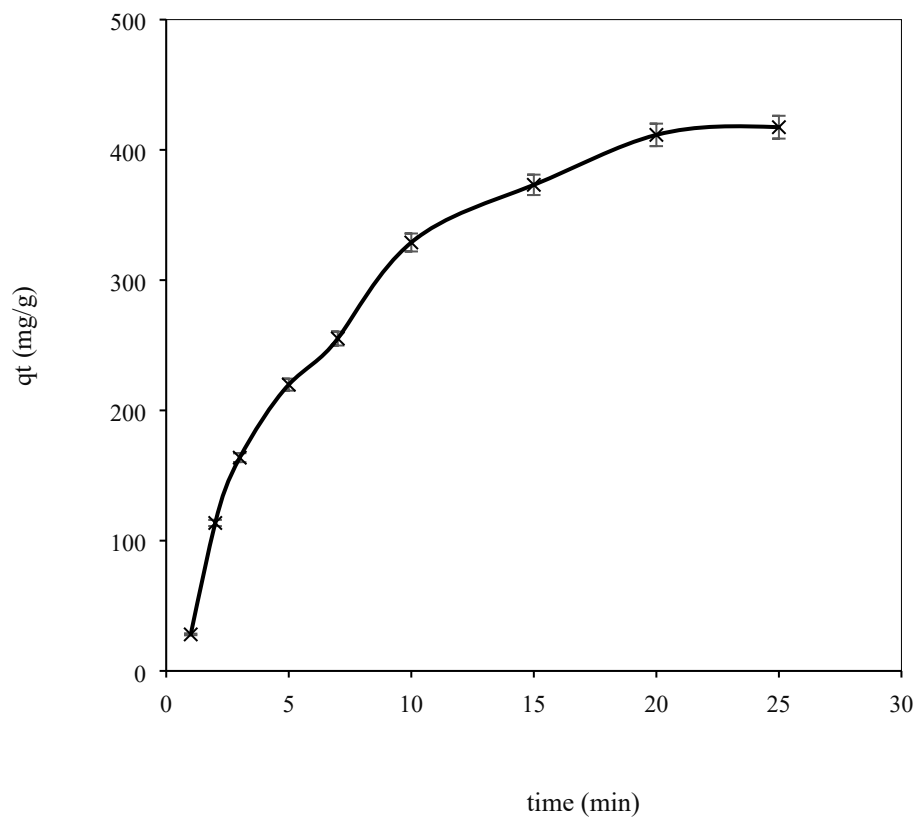


Figure S7. The effect of time on the q_t (RSD% =2.1)

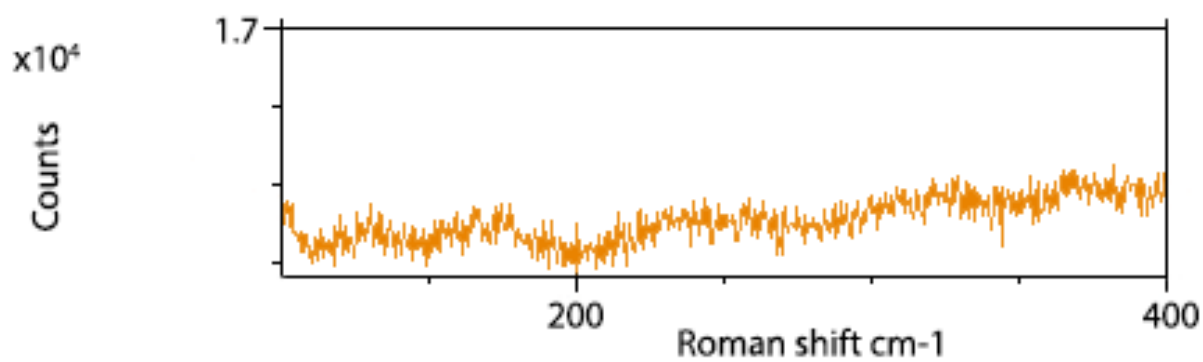


Figure S8. Raman spectra of POP-AO after iodine adsorption.

Table S1. Optimization of desorption conditions for iodine from adsorbent.

NaCl Concentration (mol/L)	Desorption time (h)	Desorption Efficiency (%)
0.5	0.5	69.3
0.5	1.0	76.5
0.5	1.5	84.2
0.5	2.0	88.6
0.5	3.0	89.1
1.0	0.5	81.4
1.0	1.0	90.3
1.0	1.5	94.1
1.0	2.0	95.8
1.0	3.0	95.9
1.5	0.5	84.1
1.5	1.0	91.6
1.5	1.5	94.5
1.5	2.0	95.8
1.5	3.0	96.1